Taylor & Francis
Taylor & Francis Group

Automatika

Journal for Control, Measurement, Electronics, Computing and Communications

ISSN: 0005-1144 (Print) 1848-3380 (Online) Journal homepage: http://www.tandfonline.com/loi/taut20

An improved startup mode using clutch coupling for in-wheel electric vehicle drives

Ping Xiong & Chenglin Gu

To cite this article: Ping Xiong & Chenglin Gu (2017) An improved startup mode using clutch coupling for in-wheel electric vehicle drives, Automatika, 58:1, 97-110, DOI: 10.1080/00051144.2017.1361612

To link to this article: https://doi.org/10.1080/00051144.2017.1361612

AUTOMATIKA, 2017
VOL. 58, NO. 1, 97–110
https://doi.org/10.1080/00051144.2017.1361612

Taylor & Francis
Taylor & Francis Group

REGULAR PAPER

OPEN ACCESS Check for updates

An improved startup mode using clutch coupling for in-wheel electric vehicle drives

Ping Xiong and Chenglin Gu

School of Electrical and Electronic Engineering, Huazhong University of Science & Technology, Wuhan, Hubei, P.R. China

ABSTRACT

By introducing a new type of clutch into the driveline system of an in-wheel drive electric vehicle, a flexible connection has been developed to replace the rigid one between the hub and the motor. The driving motor can realize variable idling, unlike the internal combustion engine, which needs a minimum rotational speed. This paper proposes a new startup method that utilizes the initial kinetic energy of the motor to achieve a smooth and fast acceleration of the wheel speed from zero to the expected motor speed. First, the powertrain system, including the driving motor, the clutch and the vehicle resistance, is modelled. Second, factors influencing the starting current and the jerk level during the starting process are investigated. In consequence, the idle speed can be interpreted as a tunable variable that determines the tradeoff between the torque capacity and the jerk level. Finally, simulation and experiments on a laboratory test rig are performed. The results validate that the proposed variable-idle speed control strategy has a lower jerk level and lower starting current when compared with those using a direct start under the same load condition.

ARTICLE HISTORY
Received 30 September 2016
Accepted 20 July 2017

KEYWORDS
Clutch coupling; startup mode; variable-idle speed; vehicle jerk

1. Introduction

The increasing awareness regarding air pollution and the energy crisis draws the attention of many researchers to the development of alternative-fuel vehicles [1]. Different kinds of green cars (e.g. hybrid electric vehicles, fuel-cell vehicles and pure electric vehicles) have been widely promoted in recent years. Although the traditional centralized-drive mode is adopted in most of them, the in-wheel drive mode is currently considered to be an attractive candidate for the electric vehicle (EV) propulsion system because of its prominent advantages, such as lower drivetrain losses, a lightweight body structure, high energy efficiency and low road noise [2,3].

The force that resists wheel motion is mainly caused by factors such as deformations of the wheel and the roadbed, bearing losses, and slippage between the wheel and the surface. The problem of vehicle startup becomes prominent, especially taking into account the additional resistance forces arising from the static friction of bearings or the relative micro-sliding between the surfaces of contact [4,5]. In the case of a vehicle starting from a dead stop, the resistive force caused by the bearing friction can actually be a larger portion of the vehicle's total rolling resistance [5]. Thus, more power is required to accelerate the wheel from a standstill, i.e. the larger driving torque of the motor has to be guaranteed when the motor is rigidly connected to the stationary driveline of the vehicle. Additionally, the voltage surge that results from the higher di/dt may damage the components, such as the Hall sensors and the controllers, if the EV brakes at a high speed [6]. Therefore, unsatisfactory starting performance and uncomfortable feelings to drivers will be inevitably produced with a rigid connection between the hub and the motor, in particular during the starting and braking processes.

Combined with the advanced control strategy, the clutch mechanism has been commonly used in the driveline of internal combustion engine vehicles and hybrid electric vehicles for reducing mechanical shock and improving the comfort level when starting the vehicle or shifting gears [7,8]. It is also applied to decrease the electromagnetic impulsion in the starting of the motor. A centrifugal clutch is used to assist with motor starting. The basic operating principle is to employ centrifugal force to engage or disengage automatically from the load at a certain rotating speed, which will result in a reduction in the residence time of electromagnetic impulsion and accumulated heat in the armature winding during the starting process [9]. Additionally, the permanent magnet (PM) coupling is considered a solution for oversizing the driving motor, especially for the starting of large-inertia equipment [10]. In addition, the dog clutch has been adopted and tested within an electric drivetrain to verify the effectiveness of the energy savings by disengaging the propulsion motor from the wheels during coasting events [11].

CONTACT Ping Xiong xping@hust.edu.cn

As stated above, the value of including the clutch mechanism within the drivetrain is examined. Several types of clutch mechanisms have been reported in literatures so far. Most of them are concerned with a mechanically controlled clutch or a centrifugal clutch mechanism concentrated mainly on the centralized-drive conditions [8,12]. However, there seem to be few references regarding the utilization of the clutch mechanism for the application of an in-wheel drive EV. Several cases have been covered in references or patents concerning the so-called "pulse and glide" driving strategy and the optional switch between a pedal drive or a motor drive in the motorized bicycle drive system [11,13], in which the dog clutch or the overrun clutch is used to disengage the propulsion motor from the wheel load.

Therefore, a new type of clutch is especially designed for the restricted space between the hub and the motor. Its operating principle and design rules were investigated in previous work [14]. As shown in Figure 1(a), the armature is polarized when the control coil is energized. Acted upon by the resultant electromagnetic force of the PM on one side, the armature is moved to the other side. Then, the clutch accomplishes the transfer from open to locked state. Accordingly, the driving torque is transmitted to the wheel after the push rods slide into the joint holes, as displayed in Figure 1(b). The push rod of the clutch functions as a torque transfer medium for the driveline system.

By applying either the friction pairs or the dog clutch pairs that are placed, respectively, at the wheel hub and the motor side, different assemblies of the clutch units can be achieved. One demonstration is shown in Figure 1(b). Several joint holes providing a uniform division of a circle are laid at the wheel hub and they correspond to the clutch's push rods. Composed of several clutch units that are uniformly mounted on the external surface of the hub motor, the actuator functions like a dog clutch for the power transmission and interruption between the motor (driving end) and the wheel (driven end) of an in-wheel electric drive system.

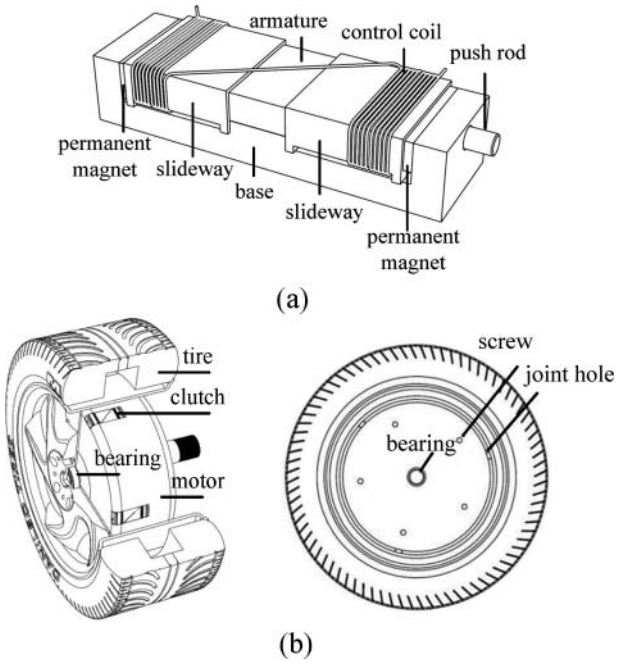

Figure 1. Schematic diagram of the assembly of clutch units between the hub and the motor in an in-wheel drive system: (a) a new type of clutch unit, (b) demonstration of the assembly of clutch units between the hub and the motor in an in-wheel drive system.

As key parts of the clutch system, this paper mainly focuses on the startup method highlighted by "no-load starting" and "variable-idle shifting" together. Based on the behaviour of an instantaneous engagement process between the motor and the wheel, the paper proposes an ideal clutch model that complies with the principle of conservation of angular momentum, which is distinguished from the control of the pressure or the displacement profile of the clutch. Accordingly, the no-load speed of the motor, i.e. the so-called idle speed, is chosen, aiming at balancing the jerk level and the starting current based on load conditions. The startup of the EV with a rigid connection between the motor and the hub is referred to as "direct start". Correspondingly, the separated process of motor startup and load operation is referred to as "clutch start".

2. Modelling the powertrain

The simplified powertrain of the in-wheel drive system presented in the article consists of three parts: the driving motor, the clutch and the vehicle resistance. Some assumptions are made before modelling. Ignoring the wheel slip, the vehicle mass can be regarded as a concentrated mass referred to the rotational shaft of the driving motor.

2.1. Modelling of the driving motor

Because the motor selection will have little effect on performance comparisons between the direct start and the clutch start, a DC motor is chosen as the main power unit of the driveline system to simplify the analysis. The DC drive system model is composed of an electrical equation and a mechanical equation,

$$L_a \frac{di_a}{dt} + i_a R_a + E = u_a, \tag{1}$$

$$J_e \frac{d\omega_e}{dt} = T_e - T_M, \tag{2}$$

where R_a is the armature resistance, L_a is the armature inductance, i_a is the armature current, ω_e is the mechanical angular speed, u_a is the input voltage, J_e is the motor inertia, T_e is the output torque of the electric machine, T_M is the load torque, and E is the back EMF

(electromotive force), which is described by

$$E = K_e \omega_e, \tag{3}$$

where K_e is the EMF constant of the electric motor.

2.2. Modelling of the vehicle dynamics

The resistive force acting upon the vehicle is generally the summation of the aerodynamic drag, rolling resistance, inclination force and acceleration [15]. Ignoring the rotational parts of the wheel, the vehicle mass is lumped into a single inertia referred to the rotational shaft of the driving motor,

$$J_v = M_v r_w^2 / G^2, \tag{4}$$

where M_v is the gross mass including the load, r_w is the tire radius, J_v is the equivalent moment of inertia referred to the rotational shaft of the driving motor, and G is the gear ratio, which has a value of 1 in direct-drive mode.

Additionally, air resistance is small enough to be ignored because the vehicle speed remains fairly low at the initial instant of startup. Combined with the electrical and mechanical equations of the DC motor, the following equations show the overall model of the direct-drive EV system:

$$\begin{aligned} &L_a \frac{di_a}{dt} + i_a R_a + K_e \omega_e = u_a \\ &\left(J_e + M_v \frac{r_w^2}{G^2}\right) \frac{d\omega_e}{dt} = K_T i_a - \frac{r_w}{G}\left(f_r M_v g + M_v g \sin\theta\right), \end{aligned} \tag{5}$$

where g is the acceleration of gravity, f_r is the coefficient of rolling friction, θ is the inclination angle, and K_T is the torque constant of the DC motor.

The resistance torque applied to the wheel on level ground is always influenced by the rolling loss group, which is attributed to factors such as the bearing losses and the deformation between the wheel and the roadbed surface. Based on the variation law of the friction coefficient of the bearing, the friction coefficient tends to have a relatively high value when the vehicle travels at a low driving speed or accelerates from a standstill [16]. Additionally, the rolling resistance is likewise the result of deformations occurring at the point of contact between the tire and the road. Road roughness will influence the tire–road frictional behaviour, and it raises static resistance with little effect on dynamic resistance [17]. Therefore, the effects of bearing friction and the tire–road frictional behaviour should be distinguished between the rolling and non-rolling situations. In some cases, the total resistance torque acting upon the wheel at the initial instant of startup could be several times larger than the one when the wheel rolls at a steady speed [16,18].

In general, the frictional behaviour of contact surfaces is often modelled as a basic Coulomb friction model, a static-kinetic friction model, or a stick-slip friction model [4]. In consideration of the complexity of characterizing the nonlinear frictional properties with an expression that should be determined through extensive experiments on a test vehicle, the static-kinetic friction model is taken into account in this article. Namely, a constant dynamic coefficient operates at all rolling speeds, whereas a higher static coefficient operates at the beginning. The symbol f_s, which corresponds to the force to start motion, would represent the static coefficient of rolling friction. Correspondingly, the symbol f_r would represent the dynamic coefficient, which is operative for the moving condition [19].

2.3. Modelling of sudden clutch engagement

By implementing the clutch start, there exists a speed difference between the motor and the wheel before the clutch engages. Two possible scenarios are distinguished during the starting period and are described as the synchronizing and engaged phases. The dynamic process of clutch engagement during the synchronizing phase can be presented as

$$J_e \dot{\omega}_e = T_e - T_c, \tag{6}$$

$$J_v \dot{\omega}_v = T_c - T_L, \tag{7}$$

where T_c is the clutch torque, ω_v is the angular speed of the wheel, and T_L is the total resistance torque acting on the wheel.

Acted upon by the clutch torque T_c, the motor speed is decreased while the wheel speed is increased. Accordingly, the motor speed during this phase is governed by the following equation:

$$\int_0^{t_c} (T_e - T_c) dt = \int_{\omega_0}^{\omega_1} J_e d\omega, \tag{8}$$

whereas the wheel speed is governed by

$$\int_0^{t_c} (T_c - T_L) dt = \int_0^{\omega_1} J_v d\omega, \tag{9}$$

where ω_0 is the no-load angular speed of the motor, ω_1 is the angular speed at the clutch lockup instant, and t_c is the elapsed time for the clutch engagement.

The angular impulse is the time integration of the torque. The impulse that is produced by the driving torque and the clutch torque will act upon the motor, while the loading torque and the clutch torque will act upon the wheel. Based on the principle of impulse, the action of the impulse can be equivalent to an average torque by the time during which it acts. Once the speed difference between the motor and the wheel

approaches zero, the clutch has been transitioned into the locked state from the open state. Then, the elapsed time for the clutch engagement can be calculated by

$$t_c = \frac{\omega_0 J_e J_v}{J_v(T_c - T_e) + J_e(T_c - T_L)}. \quad (10)$$

Moreover, in the numerical and experimental measurements carried out in [20,21], the action of rapid clutch engagement always produces high driveline loads over a short duration in the engine mounts and driveline components. In this case, supposing the equivalent clutch torque is far greater than the motor torque and the resistance torque, Equation (10) can be reduced to the following equation:

$$t_c \frac{T_c}{J_v} = \frac{J_e \omega_0}{J_e + J_v}. \quad (11)$$

It is noted from Equation (11) that the variation of wheel speed during this phase is simply proportional to the zero-load speed ω_0.

Furthermore, a rigid connection is made between the wheel and the motor while the clutch remains in a locked state, and while in an open state it transmits zero force (or torque). Analogous to ideal electrical switches, it is assumed that the ideal mechanical coupling between two masses rotating at different speeds engages or disengages instantaneously. Hence, the paper treats such an event as a completely inelastic collision, and the principle of conservation of angular momentum is applied to calculate the collision speed [22]. The common angular speed when the clutch is instantly locked is governed by

$$\omega_1 = \frac{J_e \omega_0}{J_e + J_v}. \quad (12)$$

Equation (12) implies that the common angular speed ω_1 obtained by the ideal mechanical coupling agrees with the result of the left-hand side of Equation (11). The action of rapid engagement of the clutch can be considered to be in accord with an ideal clutch that can instantaneously open or close. Additionally, the derived equation as shown in Equation (11) notes that common angular speeds are obtained by the motor and the wheel via the operation of rapid engagement of the clutch. Then, the wheel is flexibly coupled to the motor, behaving like a linking element. The single-degree-of-freedom (single-DOF) dynamic model of the clutch at the engaged phase is presented as

$$T_e - T_L = (J_e + J_v)\frac{d\omega_e}{dt}. \quad (13)$$

In [4], a typical response of the wheel moment and the wheel angular velocity is measured during a "snap-start" experiment with a standing and rolling start. It is indicated that there is a transient process with high peak values of oscillations, and the peak value of the wheel moment in the case of a standing start is higher than that in the case of a rolling start. In addition, the increase of wheel speed will help to reduce the free rolling resistance force and wheel sinkage [23]. To some extent, the required tractive torque for accelerating the wheel from a standstill would be decreased as a result of the initial speed obtained by the wheel via the operation of sudden engagement of the clutch.

3. Variable-idle speed control strategy for vehicle startup

3.1. Performance indices

The criterion for evaluating the comfort level of vehicle startup or shifting is susceptible to the subjective perception of human beings. In general, the change rate of acceleration reflects the force variation on an object, which exactly accounts for the phenomenon of the "head nod" effect on passengers during vehicle shifting or the sense of uncomfortable feelings in the case of elevator starting and stopping. Neglecting the vertical and lateral vibrations, the change rate of the vehicle's longitudinal acceleration, called jerk, is considered as the objective index of driving comfort [24]. Uncomfortable physiological feelings will be experienced as long as the absolute value of the jerk level is beyond the recommended value of 10 m/s^3 [25]. In addition, the peak armature current and the armature heating during the starting process are seen as the performance indices for quantifying the level of electromagnetic impulsion.

3.2. Determination of the idle speed for the improvement to performance indices

The minimum rotational speed of the engine, which is approximately 10%–15% of its maximum speed, is generally sufficient to assure an acceleration of the wheel speed from zero to engine speed under normal driving conditions [26]. Similarly, the same ratio of a motor's rated speed is matched with its fixed idle speed. However, because of the limitation of the starting torque of the driving motor when it is engaged to the wheel at a fixed idle speed, potential negative acceleration of the wheel would occur after the rapid clutch engagement. Therefore, the variable-idle speed control scheme is proposed to find a balance between the reduction in jerk level and the improvement of torque capacity. The specific flowchart for variable-idle speed control strategy is shown in Figure 2.

In practical applications, the initial force that resists wheel motion, i.e. the starting resistance, can be approximately estimated from the sensors or the initial

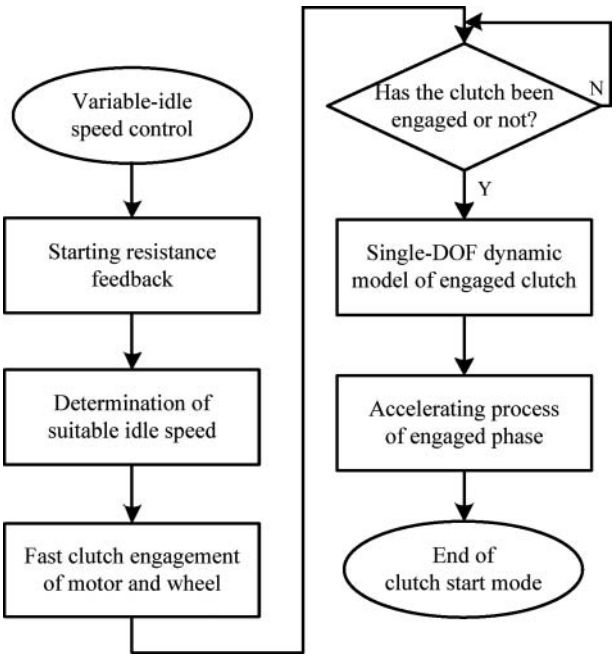

Figure 2. Flowchart of the variable-idle speed control strategy.

brake pedal displacement when the vehicle is launched from a standstill. When implementing the proposed method, the reference idle speed is tuned with the resistance force feedback before the clutch engages. Accordingly, the determination of the suitable idle speed is studied, as shown in the next subsections. After the clutch is locked, the wheel creeps at idle speed until the accelerator pedal is pressed.

3.2.1. Factors influencing the starting performance indices

Based on the analysis for the transient engaging process of the "snap-start" event, the rapid clutch engagement between the motor and the wheel in the motor–clutch–load system can be considered to comply with the law of conservation of momentum and the impulse theorem. Accordingly, the equivalent angular acceleration of the wheel is calculated as

$$\frac{\Delta\omega_{\mathrm{v}}}{\Delta t}=\frac{\overline{T}}{J_{\mathrm{v}}}, \tag{14}$$

where $\overline{T}$ is the equivalent average torque, Δt is the clutch engagement time, and $\Delta\omega_{\mathrm{v}}$ is the variation of angular velocity of the wheel.

Because the wheel speed starts from zero, its change in angular speed is defined by Equation (12). Substituting the wheel speed from Equation (12) into Equation (14), the equivalent angular acceleration of the wheel is obtained. Then, combining the definition of jerk, the transient jerk for preserving a good driving comfort at the starting time is expressed as

$$|\dot{a}|=\left|\frac{\mathrm{d}a}{\mathrm{d}t}\right|=\frac{J_{\mathrm{e}}}{J_{\mathrm{e}}+J_{\mathrm{v}}}\frac{r_{\mathrm{w}}\omega_0}{\Delta t\cdot\Delta t_{\mathrm{s}}}\le const, \tag{15}$$

where Δt_{s} is the time interval, $\dot{a}$ is the change rate of acceleration, and *const* is a constant that corresponds to the recommend jerk level.

It is concluded that human beings are generally more sensitive to the longitudinal oscillations in the frequency range around 10–14 Hz [27], while not to the ones above 50 Hz. Furthermore, the differentiation of a filtered acceleration signal with the sampling frequency of 100 Hz is used to quantify the comfort level during starting and shifting processes in a test hybrid electric vehicle [28]. For this reason, the acceleration data are sampled with the frequency of 100 Hz, and the jerk level is derived by dividing the equivalent acceleration by the time interval Δt_{s} (0.1 s) because this practice will not bring very high-frequency contents.

On the other hand, because the action of rapid clutch engagement can be regarded as the ideal clutch model, it is treated as a perfectly inelastic collision. The motor speed is rapidly decreased while the wheel speed is increased during the synchronizing phase; therefore, Equation (6) is simplified as

$$-T_{\mathrm{c}}=J_{\mathrm{e}}\frac{\mathrm{d}\omega_{\mathrm{e}}}{\mathrm{d}t}. \tag{16}$$

Accordingly, the armature current starts to increase from the no-load current to the expected load current. Combining Equation (1), Equation (12) and Equation (16), the analytical solution to the armature current can be calculated by

$$\begin{cases} i_{\mathrm{a}}(t)=R_{\mathrm{a}}^{-1}\left[\mathrm{A}t+(\mathrm{B}-\mathrm{A}\tau_a)\left(1-\exp\left(-\dfrac{t}{\tau_a}\right)\right)\right], \\ \mathrm{A}=K_{\mathrm{e}}\dfrac{\omega_0-\omega_1}{\Delta t},\ \mathrm{B}=u_{\mathrm{a}}-K_{\mathrm{e}}\omega_0 \end{cases} \tag{17}$$

where τ_{a} is the constant of electromagnetic time. Ignoring the influence of the armature reaction, the output torque of the driving motor is proportional to the armature current.

In general, the electromagnetic transient process is faster than the dynamic process of the mechanical inertia. Moreover, the variation of the armature current will respond to the wheel speed change after the clutch is engaged. Thus, the ideal clutch is locked before the electromagnetic transient process ends. Accordingly, a minimal idle speed for assuring continuous acceleration of the wheel will be obtained when the engagement time is equal to the time duration of the electromagnetic transient process.

3.2.2. Control objective

The motor torque is directly transmitted through the driveline to the wheel after the clutch is locked, whereas the clutch torque is applied to the wheel

during the synchronizing phase. Obviously, there is a sudden change in the clutch torque at speed synchronization instant, and the discontinuity in angular acceleration of the wheel at the clutch lockup time instant $\bar{t}$ is proportional to the slip angular acceleration just before the clutch is locked according to [29],

$$\begin{cases} \dot{\omega}_{\mathrm{v}}(\bar{t}^{+}) - \dot{\omega}_{\mathrm{v}}(\bar{t}^{-}) = \dfrac{J_{\mathrm{e}}}{J_{\mathrm{e}} + J_{\mathrm{v}}} \dot{\omega}_{\mathrm{sl}}(\bar{t}^{-}) \\ \dot{\omega}_{\mathrm{sl}}(\bar{t}^{-}) = \dot{\omega}_{\mathrm{e}}(\bar{t}^{-}) - \dot{\omega}_{\mathrm{v}}(\bar{t}^{-}) \end{cases}, \tag{18}$$

where $\dot{\omega}_{\mathrm{sl}}(\bar{t}^{-})$ is the slip angular acceleration before the clutch is locked, $\dot{\omega}_{\mathrm{v}}(\bar{t}^{-})$ and $\dot{\omega}_{\mathrm{v}}(\bar{t}^{+})$ are the angular accelerations of the wheel at the time instant of clutch pre-lockup and post-lockup, i.e. the time prior to the clutch lockup time instant is referred to as the pre-lockup phase, whereas the time after that is referred to as the post-lockup phase, and $\omega_{\mathrm{e}}(\bar{t}^{-})$is the angular speed of the driving motor just before the clutch is locked.

For the same time interval, the jerk level amounts to the discontinuity of the wheel acceleration. Given that the angular speed variation of the motor is far larger than that of the wheel over the same time span, the discontinuity in angular acceleration of the wheel at the clutch lockup time instant can be approximately equivalent to the jerk level while the clutch instantaneously engages. In comprehensive consideration of (15) and (18), the idle speed should be restricted to a certain range for ensuring the discontinuity of the wheel accelerations both before and after the clutch lockup time.

Because the higher rotational speed difference between the motor and the wheel will adversely affect the comfort level, the driving comfort and the motor torque requested for the continuous acceleration of the wheel are the contradictory elements. In a realistic startup strategy, the objective of the proposed strategy is naturally described as follows: the closed-form idle speed control based on the actual load conditions is to prescribe the balance between the requested motor torque and the jerk reduction. A schematic view of this principle is shown in Figure 3, where the dashed thinner line represents the inappropriate idle speed selection, which leads to a negative acceleration of the wheel after clutch engagement. In contrast, the solid thicker line represents the adjustable idle speed for assuring continuous acceleration of the wheel. In Figure 3, wheel deceleration would appear at clutch post-lockup phase when the total resistance torque is not balanced after clutch engagement, i.e. the armature current at the time instant of clutch post-lockup is lower than the load current $i_{\mathrm{a}}(\bar{t}^{+}) < I_L$.

3.2.3. Optimal principle of the idle speed control strategy

For a typical clutch engagement process, two phases are distinguished. Assuming a sudden increase in

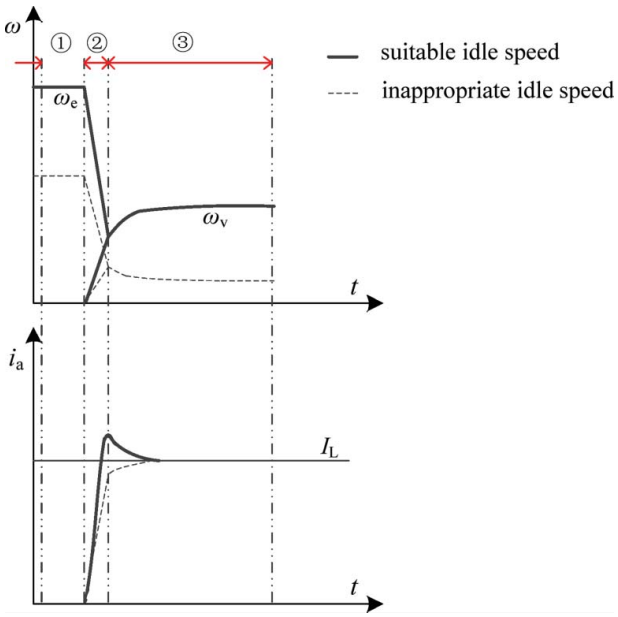

Figure 3. Comparison of the continuous and non-continuous accelerations of the wheel during the starting process: ① the phase when the motor idles at the no-load speed, ② rapid engagement of the clutch, ③ accelerating process of the engaged phase.

wheel speed is caused in the time interval $[t_0, \bar{t})$, where t_0 denotes the time instant when the motor begins to be coupled to the wheel. Ideally, the two rotating masses will turn into one linked mass once the speed difference between the motor and the wheel approaches zero, and driving with the locked clutch for $t > \bar{t}$. $a(t_0)$ is assumed to be the equivalent acceleration of the wheel by ideal coupling in the time interval $[t_0, \bar{t})$, whereas $a(\bar{t})$ stands for the wheel acceleration at the clutch lockup time instant.

Based on the ideal clutch model, the equivalent angular acceleration of the wheel is determined by Equation (14). The corresponding wheel acceleration when the clutch instantaneously engages is calculated as

$$a(t_0) = \frac{r_w J_e}{J_e + J_v} \frac{\omega_0}{\Delta t}. \tag{19}$$

Equation (19) shows that $a(t_0)$ is proportional to the idle speed. While the motor torque is directly transmitted to the wheel once the clutch is locked, the wheel acceleration at the time instant of clutch post-lockup is determined by Equation (13) and calculated as

$$a(\bar{t}^{+}) = r_w \frac{K_T i_a(t) \mid_{t=\Delta t} - T_L}{J_v + J_e}, \tag{20}$$

where $i_{\mathrm{a}}(t)$ is given by Equation (17).

As shown in Equation (20), the magnitude of the output torque of the motor at clutch post-lockup instant, under the same load condition, has a direct effect on the slope of the wheel acceleration at clutch

post-lockup instant. Therefore, the slope of this acceleration–speed relationship ($a(\bar{t}^+) - \omega_0$) is equal to the slope of torque–speed relationship ($T_e(\bar{t}^+) - \omega_0$). Moreover, the response of the armature current shown in Equation (17) implies that the output torque of the motor at $\bar{t}$ is a linear function of the idle speed, and the slope of it versus the idle speed is positive. It can be inferred from Equations (19) and (20) that the wheel accelerations, respectively, at clutch pre-lockup and post-lockup phases increase along with the rise of the idle speed. Accordingly, two cases regarding the different slope of the wheel accelerations at the pre-lockup and post-lockup phases are respectively considered. Figure 4 shows the representation of the wheel accelerations at the post-lockup and pre-lockup phases based on different idle speeds.

When the slope of $a(\bar{t}^+)$ is more than the one of $a(t_0)$, as shown in the shaded region of Figure 4(a), the absolute value of variation in wheel acceleration at the clutch lockup instant gradually decreases with the rise of the idle speed if $a(\bar{t}^+) < 0$, i.e. the motor torque at the clutch post-lockup time instant is lower than the load torque,

$$\underset{\omega_0}{|\, a(\bar{t}^+) - a(t_0) \,|} > \underset{\omega_0+\Delta\omega}{|\, a(\bar{t}^+) - a(t_0) \,|} \quad if\ T_e(\bar{t}^+) < T_L. \tag{21}$$

Moreover, regarding the negative wheel acceleration that occurs at the time instant of clutch post-lockup, it will lead to $|a(\bar{t}^+) - a(t_0)| > |a(t_0)|$. By assuming that the lockup phenomenon has a finite time duration, the discontinuity of the wheel acceleration is interpreted as an approximation of the jerk caused by the clutch lockup. Therefore, a larger absolute value of the jerk level is obtained at the clutch post-lockup phase, compared with the transient one while the clutch instantaneously engages. The major jerk level during the starting process is governed by $|a(\bar{t}^+) - a(t_0)|$ in the shaded region of Figure 4(a).

On the other hand, when the motor torque requested for the non-negative acceleration at the time

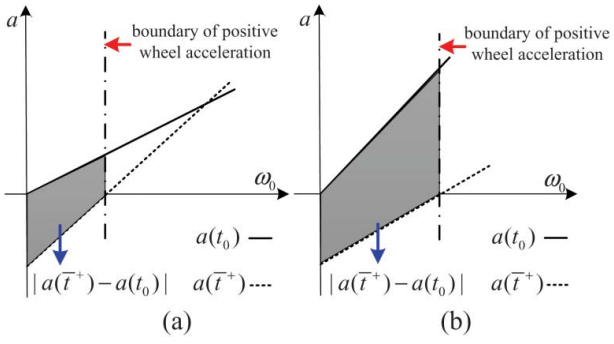

Figure 4. Graphical illustration of the wheel accelerations at the clutch post-lockup and pre-lockup phases with different idle speeds.

instant of clutch lockup is guaranteed, i.e. $a(\bar{t}^+) > 0$, as shown in the region on the right side of the shaded area of Figure 4(a), the max discontinuity of the wheel acceleration $\Delta a_{\max}$ during the starting process is governed by

$$\underset{[t_0,\, \bar{t}^+]}{\Delta a_{\max}} = \begin{cases} a(t_0) & \text{if } |\, a(\bar{t}^+) - a(t_0) \,| < a(t_0) \\ a(\bar{t}^+) - a(t_0) & \text{if } |\, a(\bar{t}^+) - a(t_0) \,| > a(t_0) \end{cases}. \tag{22}$$

Equation (22) shows that the max discontinuity of the wheel acceleration increases with the idle speed. Combined with Equation (21), it indicates that an inflection point emerges in the max discontinuity of the wheel acceleration with the idle speed adjustment. Therefore, the minimum jerk level will be achieved in this case.

Taking the comfort level and the electromagnetic impulsion into account, the lower starting current and the smaller jerk level are usually preferred during the starting process. According to the above-mentioned analytical results, no more improvements to the jerk level can be made with the increase of the armature current overshoot. The given idle speed that corresponds to the output torque of the motor at the post-lockup time instant to balance the load torque can be interpreted as a Pareto-optimal point of the two performance indices: for a given value of load torque, or implicitly, for a given armature current, the jerk level is optimal, because of a smaller discontinuity in the wheel acceleration during the starting process.

Another case is shown in Figure 4(b). Although the absolute value of variation in wheel acceleration at the time instant of the clutch lockup increases with the idle speed during the whole starting process, there also exists an obvious change in the max discontinuity of the wheel acceleration at the critical boundary of the positive wheel acceleration. Therefore, similar to a two-point minimization technique that is used for jerk optimization, the offline optimization regarding the idle speed selection is explained as follows: as long as the adjacent difference ($jerk_n - jerk_{n-1}$) is lower than the threshold value, incrementing of the idle speed is continued. Once the difference is larger than the threshold value, incrementing of the idle speed is stopped, and the corresponding idle speed can be regarded as an optimal point under one load condition. Therefore, the adoption of this idle speed can be interpreted as an optimization process, during which the continuous wheel acceleration is achieved without inducing a fast increase of jerk level.

4. Simulation and analysis

Given that the variations of the road and load conditions are ultimately converted to the load torque

applied to the driving motor, the performance comparisons between the direct start and the clutch start are investigated under the same load condition. As the key element of an in-wheel EV drive, the hub motor is featured by high torque and low speed. First, similar to the features of a hub motor, the parameters of the driving motor are considered for an in-wheel drive condition.

In general, the rolling coefficient is approximately 0.01–0.018 under normal driving conditions. As mentioned in Section 2, taking into account the bearing friction or the complex tire–road interactions, the stationary resistance torque at the initial instant of starting can reach several times the value of the rolling one. Hence, in the case of a vehicle starting from a standstill, a working condition where the f_s is assumed to be three times as much as the f_r is considered. The simulation parameters of a lightweight EV and the driving motor are specified in Table 1.

Because the road and load conditions are widely varied, the scheme of reducing the voltage across the armature without current limiting is commonly adopted for the motor starting with the load. During this case, the peak current is governed by

$$I^*_{\max} = \frac{u^*_a}{R^*_a}. \tag{23}$$

Note that variables, respectively, with superscript * and subscript "N" stand for the per-unit value and the rated value. The average jerk value is calculated by the differentiating Equation (13) with respect to time,

$$\dot{a} = \frac{\mathrm{d}a}{\mathrm{d}t} = \frac{r_w}{J_v + J_e}\frac{\mathrm{d}T_e}{\mathrm{d}t} = \frac{r_w K_T}{J_v + J_e}\frac{\mathrm{d}i_a}{\mathrm{d}t}. \tag{24}$$

Equation (24) shows that the torque variation is equivalent to the change rate of the acceleration, which is the same as the physical significance of the jerk. Equations (23) and (24) suggest that reducing the input voltage across the armature is advantageous for decreasing the starting current and increasing the comfort level. However, it will cause a longer starting time of the motor. The wheel stays stationary until sufficient motor torque is supplied to overcome the starting resistance moment, i.e. the armature current increases to the load current I_L from the no-load current. During this phase, the response of the armature current is determined by

$$i_a(t) = \frac{u_a}{R_a}\left(1 - \exp\left(-\frac{t}{\tau_a}\right)\right). \tag{25}$$

Accordingly, the elapsed time t_d when the wheel is set into motion is governed by the solution of equation $I_L = i_a(t)$, and it is described as follows:

$$t_d = -\frac{1}{\tau_a}\ln\left(1 - \frac{T_L R_a}{u_a K_T}\right). \tag{26}$$

Because of the fact that the electrical time constant of the motor is negligibly small compared with the mechanical time constant of the driveline system, the per-unit value of total dissipated energy in the windings of the motor or equivalent heating in the armature over the starting period is determined by [30] to be

$$Q^* = \int_0^{t_r}\left[(I^*_{\max} - I^*_z)\exp\left(-\frac{t}{\tau_m}\right) + I^*_z\right]^2 \mathrm{d}t. \tag{27}$$

τ_m is the mechanical time constant of the driveline system, t_r is the elapsed time from rest to steady load speed, and I_z is the steady load current.

Next, on the premise of the minimum tractive torque to propel the vehicle into motion, the clutch start and the direct start are simulated under the same load condition for comparison. The contrast curves of the motor and wheel speeds, armature current, equivalent armature heating and jerk level are sequentially shown in Figure 5. The rated current and the recommended jerk value are the base values of the armature current and the jerk level.

As shown in Figure 5(a), the motor is idling at approximately 30 r/min (n_e) before the clutch engages. At time instant 1 s, the motor begins to connect to the wheel. Because of the significant loads for a short duration among the driveline components by the ideal engaging process, it will lead to momentum transfer from the motor to the wheel. Correspondingly, the quick deceleration of the motor is acquired while the wheel is obtained with an initial speed.

Ideally, based on the simple model as described in Section 2, the transition between the static and kinetic conditions occurs when the common speeds of the motor and the wheel are obtained by an ideal clutch. Thus, the dynamic resistance torque needs to be overcome to maintain the wheel speed in the creep mode after clutch engagement. In contrast, as indicated by Equation (26), the wheel starts rotation when the armature current rises to compensate the static

Table 1. Simulation parameters of the vehicle and the DC motor.

Name	Symbol (unit)	Value
DC motor		
Rated voltage	U_N (V)	60
Rated current	I_N (A)	56
Rated speed	n_N (r/min)	540
Armature resistance	R_a (Ω)	0.05
Inertia of motor	J_e (kg m^2)	0.5
Vehicle		
Full load gross mass	M_v (kg)	1000
Tire radius	r_w (m)	0.3
Gear ratio	G	1
Static coefficient of rolling friction	f_s	0.03
Dynamic coefficient of rolling friction	f_r	0.01

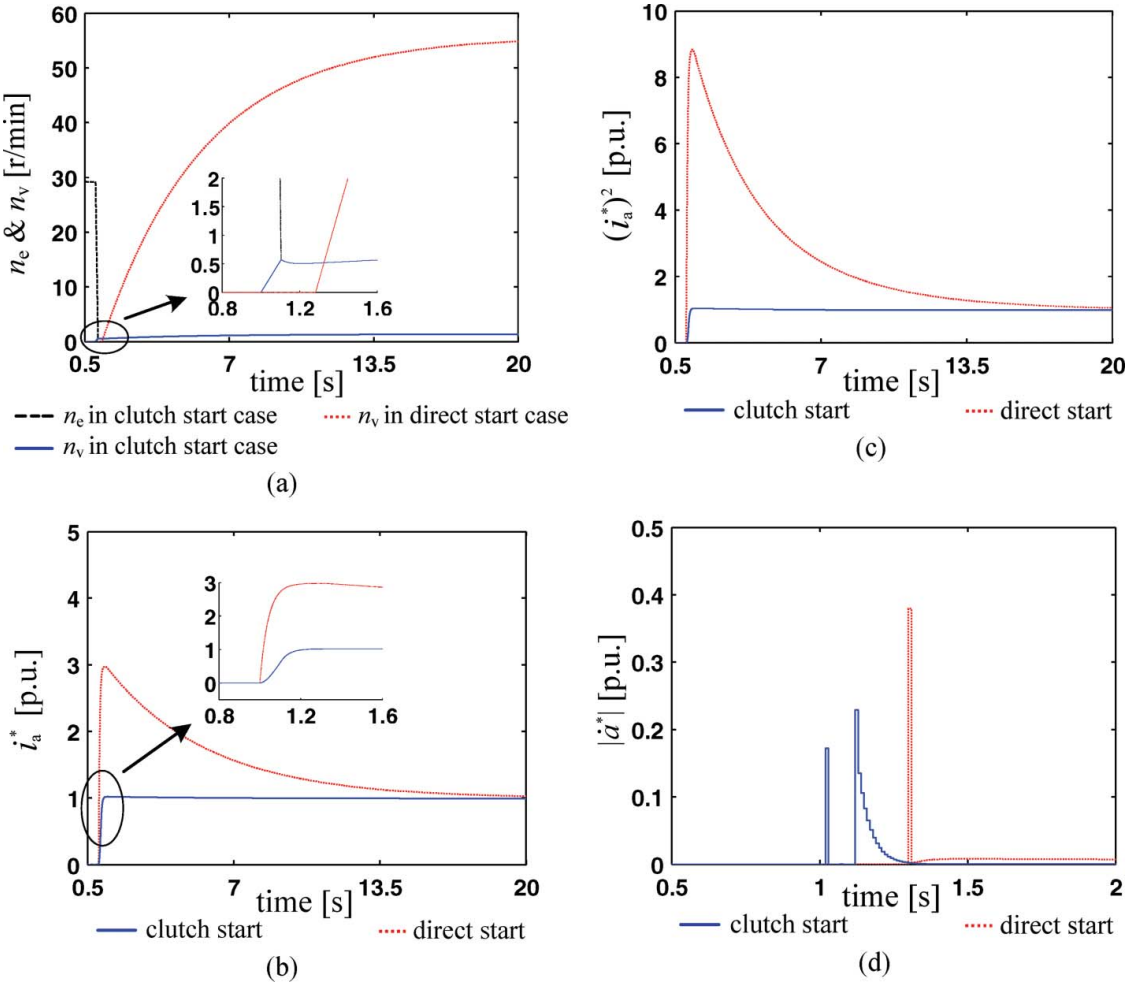

Figure 5. Comparisons between the direct start and the clutch start under the same load condition: (a) angular speed, (b) armature current, (c) equivalent armature heating, (d) jerk level.

resistance torque. As shown in the subgraph of Figure 5 (a), the speed curve displayed as a dotted line (n_v) shows that the wheel is set into motion at approximately 1.2 s. Apparently, the time instant when the wheel accelerates from zero in the direct start case lags behind that using the clutch start. On the minimum tractive torque for accelerating the wheel from a standstill, the lag time using the direct start is the right time when the armature current reaches its peak current.

During the process of the clutch start from 1 s to 20 s in Figure 5(b), the armature current rises from the no-load current to the expected load current. Figure 5(b) indicates the peak current using the direct start is three times that of using the clutch start. Additionally, in Figure 5(c), the area between the equivalent armature heating curves represents the energy reduction using the clutch start, where the energy losses are reduced by 40% during the starting period, compared with the one using the direct start. Moreover, the jerk curves using the direct start and the clutch start tend to be zero with the increase of the wheel speed. Figure 5(d) shows that the max jerk value using the clutch start is approximately 60% of that using the direct start.

Furthermore, the corresponding acceleration curve of the wheel is displayed in Figure 6. There exists a negative acceleration of the wheel during the starting process, which accounts for the larger jerk level at the clutch lockup time than the one at the time when the clutch initially engages at the speed of 30 r/min. Then, the armature current at the time instant of the clutch lockup and the max jerk level, respectively, tuned with different idle speeds are graphically demonstrated in Figure 7. An obvious change in the slope of the fitted jerk curve occurs near the idle speed at approximately 42 r/min. Figure 7 implies that the fitted jerk curve exhibits an inflection point where the output torque of the motor at the clutch lockup time is matched to the load torque at dynamic state ($T_L^* = 1$). The simulation results are basically in accord with the aforementioned analysis in Section 3.2.

5. Experiments and analysis

To validate the effectiveness of using the clutch start for reducing the mechanical and electromagnetic shocks further, as well as its optimal idle speed strategy, a set of experiments are performed on a laboratory

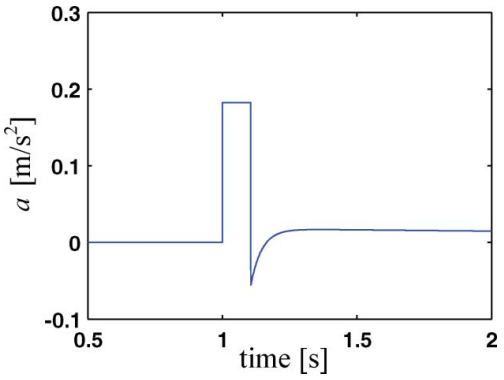

Figure 6. Plot of the wheel acceleration when the clutch engages at the speed of 30 r/min.

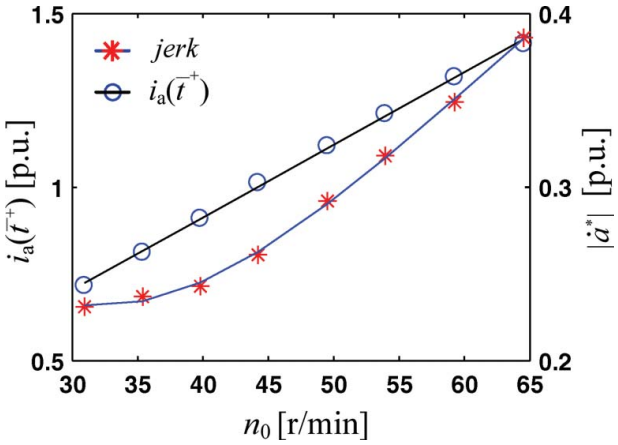

Figure 7. Plot of the armature current (p.u) at the clutch lockup time and the jerk level for the clutch start at variable-idle speeds.

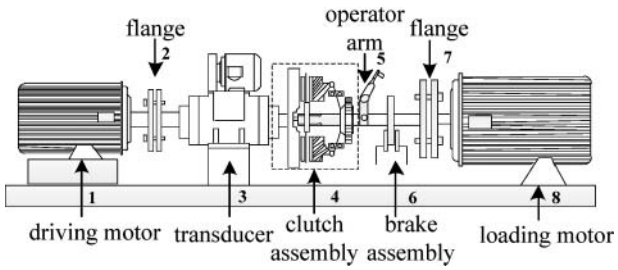

Figure 8. Description of the experimental setup.

test rig. A brief description of the experimental setup is shown in Figure 8.

5.1. Test rig

The test rig, as shown in Figure 9, is basically composed of the following parts that include the driving motor (1), flanges (2) and (7), speed and torque transducer (3), clutch assembly (flywheel, pressure plate and friction disk) (4), clutch operator (5), brake assembly (brake disk and friction pairs) (6) and loading motor (8). The driving end of the powertrain system is composed of the motor and the flywheel. The driven end is composed of the loading motor in series with the brake assembly.

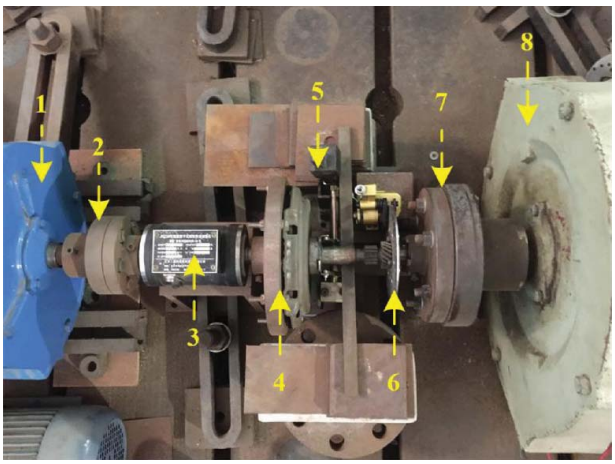

Figure 9. Photograph of the experimental setup for simulating load startup in direct-drive mode.

Because of its simple control, a separately excited DC motor is chosen as the driving unit of the driveline system. A speed and torque transducer is placed between the driving motor and the clutch assembly to measure the load torque and the rotational speed of the driving motor. A 30 kW DC motor is located at the end of the driveline, and serves as a generator and the reference moment of inertia of the load. The parameters of the driving motor and the loading motor are listed in Table 2.

For simplifying the construction of the driveline system and focusing on the regulation of the idle speed strategy, an integrated mechanical clutch is used for the power transmission and interruption and is controlled by the operator arm. The electric machine is initially increased to the expected idle speed when the clutch is in an open state. Then, for the purpose of accelerating the loading motor from a standstill, the sudden engagement of the clutch is finished by quickly releasing the pressure plate to utilize the initial kinetic energy of the driving end. In this manner, the impulse loads for a short duration that act upon the driveline components can be produced by the operation of the rapid movement of the pressure plate for locking the clutch as quickly as possible. Accordingly, the action of the angular impulse is transferred to the

Table 2. Parameters of the diving motor and the loading motor

Name	Symbol (unit)	Value
Driving motor		
Rated voltage	U_N (V)	110
Rated current	I_N (A)	35
Rated speed	n_N (r/min)	750
Armature resistance	R_a (Ω)	0.412
Field voltage	U_f (V)	220
Field current	I_f (A)	1.36
Inertia of motor	J_e (kg m^2)	0.5
Loading motor		
Rated voltage	U_N (V)	220
Rated current	I_N (A)	160
Rated speed	n_N (r/min)	1500
Inertia of motor	J_m (kg m^2)	2.6

loading motor and is equivalent to the change in angular momentum of the driving end of the powertrain system to the greatest extent possible.

Generator dynamometer is commonly used to provide motor load, but it is difficult to achieve a quick loading torque at the initial instant of startup. The brake assembly is introduced and is composed of a brake disk, a mechanical actuator and the friction pairs. It basically defines the mechanical load on the driven end of the driveline system. The static friction torque is applied to the driven end of the driveline system when contact surfaces between the friction pairs and the brake disk remain at rest, while the dynamic loading torque is produced by the relative sliding between them. Therefore, the mechanical load that is produced by using a disk brake naturally mimics the transition of resistance force from static to dynamic state during the starting process. Using this type of load imitates a condition where the resistance force is caused by the wheel bearing drag in the case of a vehicle starting from a standstill. A simplified character for the resistance force caused by the braking effect of the disk brake is followed by using the friction model reviewed in [31]. The friction force is modelled as a function of sliding velocity for a case where the static friction coefficient is larger than the dynamic friction coefficient. In this paper, the resistance force initially at rest and at a low rotating speed can be obtained using data from the test rig.

Nevertheless, the ideal clutch load transfer via the action of rapid clutch engagement and dynamic loading can be achieved on the test rig mentioned above. The existing experimental setup is still suitable for investigations on the regulation of the idle speed control strategy and for validating its effectiveness.

5.2. Comparisons and performance

In the following section, some contrast results are achieved by applying the direct start and the clutch start, respectively, on the test rig.

In general, the operating velocity of an in-wheel drive EV is not high. The max velocity of an in-wheel drive EV is roughly 50–60 km/h in consideration of the urban drive cycle. Therefore, the reference input voltage u_a is limited to 60 V to ensure that the max angular speed of the driving motor is approximately 400 r/min (50 km/h) in this paper. The load acceleration is estimated from the sampled speed signal, using a differentiator with a low-pass filter, where a cut-off frequency of 100 Hz gives a good balance between the phase lag and the noise. The base value of current is the rated current (35 A). Additionally, the equivalent jerk $\dot{a}_d$ is directly calculated by the second derivative of the sampled speed and considered for the transverse comparisons of the comfort level in the following tests.

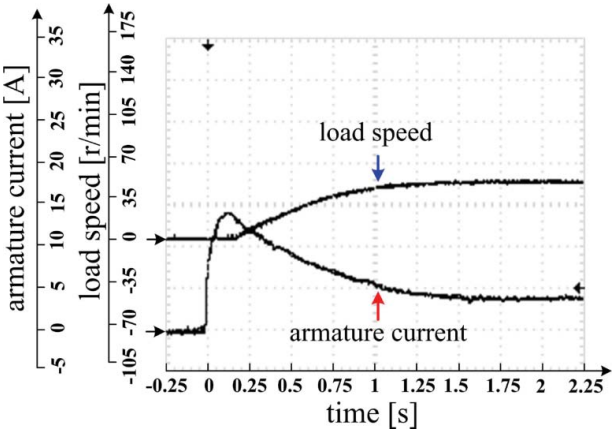

Figure 10. Scope capture using the direct start with the given armature voltage that corresponds to the fixed idle speed.

To be consistent with the ratio of the minimum stable idle speed to the max engine speed, the no-load speed of the DC motor that corresponds to 15% of the restricted voltage is considered as the fixed idle speed. Under this condition, the experiment using the direct start is then conducted. The current curve in Figure 10 suggests that the peak current is approximately three times larger than the steady-state current. Moreover, it shows that the loading motor remains at rest until the armature current rises to its peak, and the loading motor begins to accelerate from a standstill until the armature current reaches its steady-state value. It is implicitly indicated that a starting condition with static resistance moment that amounts to three times the value of the stable one is considered, under which the follow-up experiments are performed.

Then, the experiments using the clutch start are carried out when the driving motor is idling at the variable no-load angular speeds before the clutch instantaneously engages. The peak current and the max equivalent jerk at different idle speeds for the clutch start are sequentially shown in Figure 11. Similar to the proportional relationship between the idle speed and the armature current described by Equation (17), it indicates that the peak current increases linearly with the rise of the idle speed. Hence, the motor preferably idles at a smaller no-load angular speed before the clutch engages because the lower starting current will be obtained. But negative acceleration of the loading motor will occur when the motor torque at the time instant of the clutch lockup is lower than the frictional resisting moment, although the loading motor acquires a rotational speed because of momentum transfer from the driving motor. As shown in Figure 12, the load speed is gradually decreased to zero after the clutch engagement when the driving motor is idling at a speed of 22 r/min.

However, as shown in Figure 13, the creeping speed of the loading motor without rotor-lock is ensured when the clutch instantaneously engages at a speed of

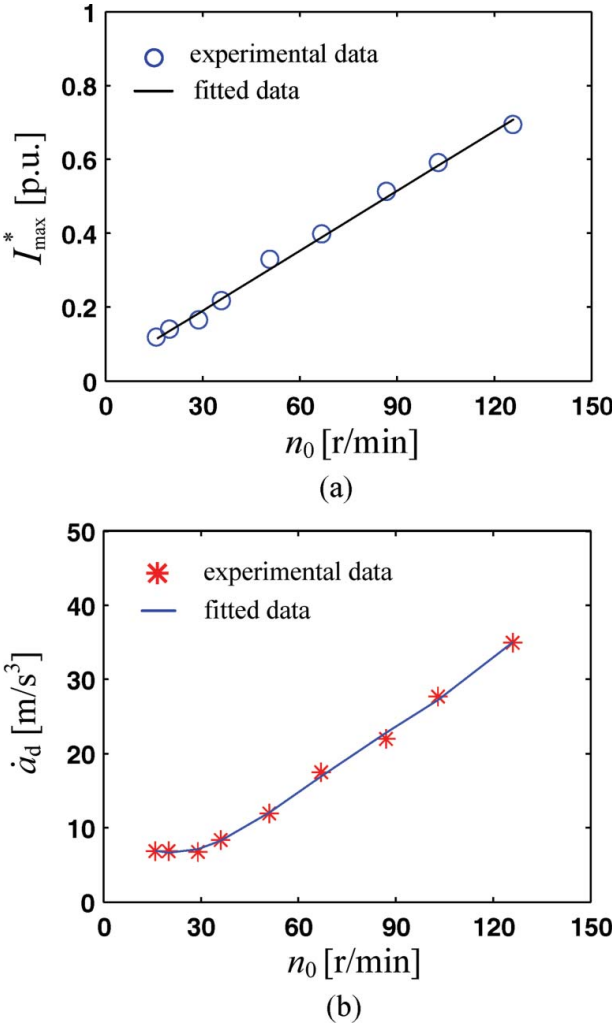

Figure 11. (a) Relationship between the idle speed and the peak armature current. (b) Relationship between the idle speed and the max jerk level.

32 r/min. Because of the different dynamic torques applied to the loading motor during the clutch engagement period, the load speed curve shows two different accelerating phases in Figure 13, and it implies that the common speeds of the driving motor and the loading motor are acquired before reaching the peak armature current. Furthermore, the value of the armature

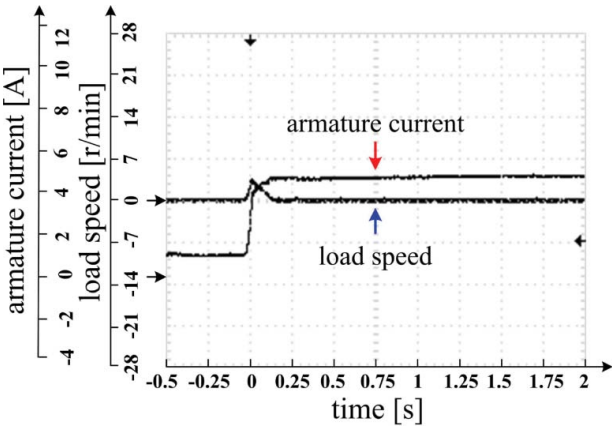

Figure 12. Scope capture using the clutch start idling at 22 r/min under steady-state load torque of 6 N m.

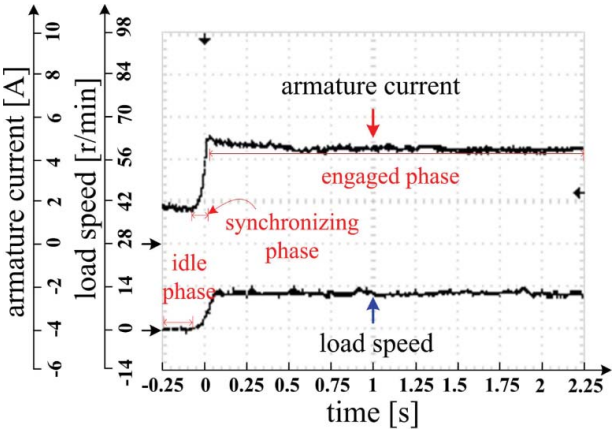

Figure 13. Scope capture using the clutch start when the clutch engages at the idle speed of approximately 32 r/min.

current at the time instant of clutch lockup amounts to that of the steady-state load current. Moreover, as shown in Figure 11(b), there is an inflection point in the plotted curve between the idle speed and the jerk level when the clutch engages at the idle speed of 32 r/min. It is implied that no more improvements can be achieved regarding the equivalent jerk while the undesired larger value of the armature current overshoot is obtained by increasing the idle speed further. On the whole, the no-load speed when the driving motor idles at a speed of 32 r/min can be interpreted as a Pareto-optimal point. The experimental results are basically in accordance with the aforementioned analysis in Section 3.

Subsequently, the contrast results between the direct start and the clutch start are shown in Figure 14. As expected, similar results are obtained as with the simulation, showing the larger value of the peak current and the jerk level by using the direct start, although fast load acceleration is obtained. Obviously, the comparison results in Figure 14(a) clearly indicate the loading motor begins to accelerate at the instantaneous time while the clutch engages, which is faster than the time instant when the loading motor accelerates from a standstill by using the direct start. Moreover, in contrast to the performance indices of using the direct start, the peak current and the max jerk value by using the clutch start are reduced approximately by 67% and 50%, as shown in Figure 14(b,d). Accordingly, the current curve by using the clutch start is a concave-upward response function, which is different from the slightly concave-downward one by using the direct start because of the influence of static resistance torque. In contrast to the case of direct start, the lower armature current is obtained by applying the clutch start, resulting in the lower armature heating over the starting period. Figure 14(c) proves the improvement of the energy reduction by using the clutch start under the same load condition. The area between the equivalent armature heating curves represents the energy reduction during the starting phase. It is clearly seen

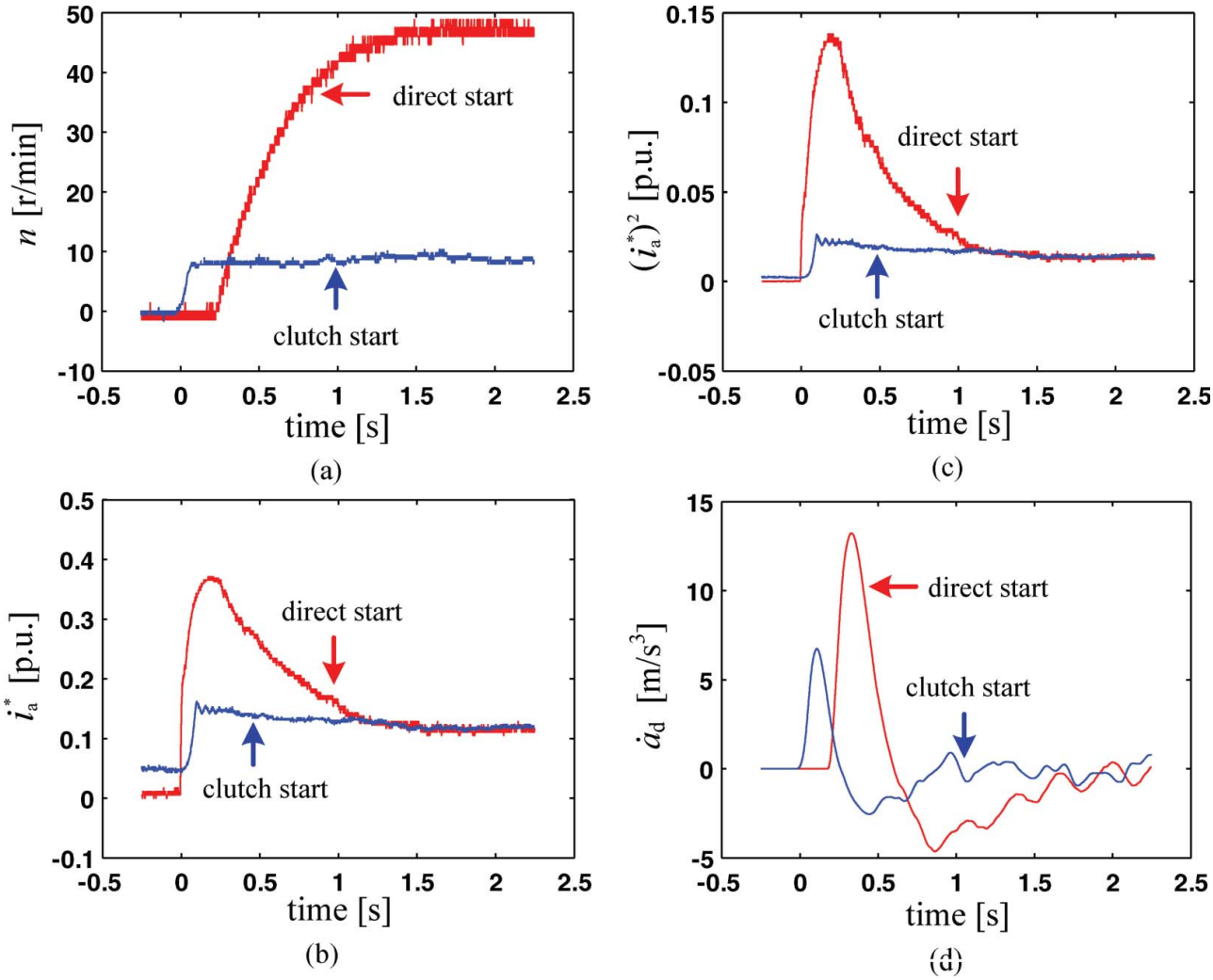

Figure 14. Experimental results of using the direct and the clutch start modes under the same load condition: (a) load angular speed, (b) armature current, (c) equivalent armature heating, (d) jerk level.

that the direct start case consumes a large amount of energy when compared with the clutch start case. The equivalent armature heating is reduced by approximately 40% by using the clutch start.

Overall, the experiments show the process for EV launch without rotor-lock can be achieved by using the clutch start. The advantages of using the clutch start over the direct start are illustrated through the experiments on the laboratory test rig, as well as the regulation method of the variable-idle speed strategy.

6. Conclusion

The startup problem of a quick and smooth clutch engagement is considered for the in-wheel EV drive that uses initial kinetic energy storage of the driving end for vehicle launch. The paper contributes a new, simple control method featured by the separated process of motor starting and load operation. The results indicate that the starting current and the per-unit value of the armature heating are decreased by approximately 67% and 40% respectively, and the comfort level is doubled compared with the direct start case under the same load condition. Apparently, the clutch start mode can be treated as an effective solution to the startup problems for an in-wheel drive electric propulsion system, because it exhibits lower starting current and higher driving comfort compared with the ones provided by using direct start. The results will be an important reference for follow-up research on the overall integration of the clutch system.

Acknowledgments

The authors would like to thank the editors and reviewers for their thoughtful comments that have significantly assisted in the improvement of this paper.

Disclosure statement

No potential conflict of interest was reported by the authors.

Funding

This work was supported by the Natural Science Foundation of China [grant number 51377063].

References

[1] Deur J, Škugor B, Cipek M. Integration of electric vehicles into energy and transport systems. Automatika. 2015;56(4):395–410.

[2] Yang YP, Liu JJ, Wang TJ, et al. An electric gearshift with ultracapacitors for the power train of an electric vehicle with a directly driven wheel motor. IEEE Trans Veh Technol. 2007;56(5):2421–2431.

[3] Ramsden VS, Mecrow BC, Lovatt HC, et al. A high efficiency in-wheel drive motor for a solar-powered vehicle. Proceedings of the IEE Colloqium on Electrical Machine Design for All-Electric and Hybrid-Electric Vehicles; 1999 Oct; London, England. London (UK): IET. p. 3/1–3/6.

[4] Maurice JP, Savkoor AR. Influence of flexibility properties and friction laws on tyre behaviour. Veh Syst Dyn. 2003;37:107–124.

[5] Heißing B, Ersoy M. Chassis handbook: fundamentals, driving dynamics, components, mechatronics, perspectives. Berlin: Springer; 2011.

[6] Gupta BK, Nilsson NE, Sharma DK. Protection of motors against high voltage switching surges. IEEE Trans Energy Convers. 1992;7(1):139–147.

[7] Lee HD, Sul SK, Cho HS, et al. Advanced gear-shifting and clutching strategy for a parallel-hybrid vehicle. IEEE Ind Appl Mag. 2000;6(6):26–32.

[8] Sporleder J, Mohlin M, Olsson M. Development of shift comfort for manual transmissions in passenger cars. ATZ Worldwide. 2008;110(6):18–24.

[9] Tan LX, Ning LW, Zhou ZR. Controlled by computer's centrifugal clutch to add power with hydraulic pressure and electromagnetism. J Mech Eng. 2003;39(12):151–153+157.

[10] Post RS. Permanent magnet coupling fundamentals. AISE Steel Technol. 1999;76(11):54–58.

[11] Camilleri R, Armstrong P, Ewin N, et al. The value of a clutch mechanism in electric vehicles. Proceedings 27th International World Electric Vehicle Symposium and Exhibition; 2013 Nov; Barcelona, Spain. Piscataway (NJ): IEEE. p. 1–11.

[12] Altendorf JP. An electric vehicle drive concept using a centrifugal clutch. Proceedings of the 14th Intersociety Energy Conversion Engineering Conference; 1979 Aug; Boston, MA, USA. New York (NY): IEEE. p. 637–642.

[13] Murphy LJ, Mirades TE. Motorized bicycle drive system. United States patent no. 5242028A. 1993.

[14] Cai WL, Gu CL, Hu XD. Analysis and design of a permanent magnet bi-stable electro-magnetic clutch unit for in-wheel electric vehicle drives. Energies. 2015;8(6):5598–5612.

[15] Lu TL, Dai F, Zhang JW, et al. Optimal control of dry clutch engagement based on the driver's starting intentions. Proc Inst Mech Eng D: J Automobile Eng. 2012;226(8):1048–1057.

[16] Manfred M, Henning W. Dynamik der Kraftfahrzeuge. Berlin: Springer; 2013.

[17] Hersey MD, Golden PL. Rolling friction. Additional car wheel experiments. J Lubric Technol Trans ASME. 1970;92(1):83–88.

[18] Ray LE. Estimation of terrain forces and parameters for rigid-wheeled vehicles. IEEE Trans Robot. 2009;25(3):717–726.

[19] Domenech A. Introduction to the study of rolling friction. Am J Phys. 1987;55(3):231–235.

[20] Kemper S, Powell N, Poggi M, et al. Modelling of snap start behaviour in an automotive driveline. Newport Beach (CA): MSCSC Software Support Library; 1999.

[21] Bingham P, Theodossiades S, Saunders T, et al. A study on automotive drivetrain transient response to 'clutch abuse' events. Proc Inst Mech Eng D: J Automobile Eng. 2016;230(10):1403–1416.

[22] Mosterman PJ, Biswas G, Otter M. Simulation of discontinuities in physical system models based on conservation principles. Proceedings of the Summer Computer Simulation Conference; 1998 July; Reno, NE, USA. San Diego (CA): SCS. p. 320–325.

[23] Shmulevich I, Mussel U, Wolf D. The effect of velocity on rigid wheel performance. J Terramech. 1998;35(3):189–207.

[24] Huang QN, Wang HY. Fundamental study of jerk: evaluation of shift quality and ride comfort. SAE Automotive Dynamics, Stability and Controls Conference and Exhibition; 2004 May; Detroit, MI, United States. Warrendale (PA): SAE International. p. 93–98.

[25] He HW, Liu ZT, Zhu LM, et al. Dynamic coordinated shifting control of automated mechanical transmissions without a clutch in a plug-in hybrid electric vehicle. Energies. 2012;5(8):3094–3109.

[26] Mollenhauer K, Tschöke H. Handbook of diesel engines. Berlin: Springer; 2010.

[27] Duan CW. Analytical study of a dog clutch in automatic transmission application. SAE Int J Passenger Cars Mech Syst. 2012;7(3):1155–1162.

[28] Zhang JZ, Lu X, Wang LF, et al. A study on the drivability of hybrid electric vehicle. 2008 SAE International Powertrains, Fuels and Lubricants Congress; 2008 June; Shanghai, China. p. 11–19.

[29] Dolcini P, de Wit CC, Bechart H. Lurch avoidance strategy and its implementation in AMT vehicles. Mechatronics. 2008;18(5–6):289–300.

[30] Sheta MA, Agarwal V, Nataraj PSV. A new energy optimal control scheme for a separately excited DC motor based incremental motion drive. Int J Autom Comput. 2009;6(3):267–276.

[31] Olsson H, Astrom KJ, De Wit CC, et al. Friction models and friction compensation. Eur J Control. 1998;4(3):176–195.